Hindawi

Research Article

Thermal Radiation and Viscous Dissipation Impacts of Water and Kerosene-Based Carbon Nanotubes over a Heated Riga Sheet

R. Prabakaran [ID],[1] **S. Eswaramoorthi** [ID],[2] **K. Loganathan** [ID],[3] **and Sonam Gyeltshen** [ID][4]

[1]*Department of Mathematics, Coimbatore Institute of Technology, Coimbatore, 641014 Tamil Nadu, India*
[2]*Department of Mathematics, Dr. N.G.P. Arts and Science College, Coimbatore, 641048 Tamil Nadu, India*
[3]*Department of Mathematics and Statistics, Manipal University Jaipur, Jaipur, 303007 Rajasthan, India*
[4]*Department of Humanities and Management, Jigme Namgyel Engineering College, Royal University of Bhutan,
  Dewathang, Bhutan*

Correspondence should be addressed to S. Eswaramoorthi; eswaran.bharathiar@gmail.com
and Sonam Gyeltshen; sonamgyeltshen@jnec.edu.bt

This research communication explains the flow of water/kerosene-based CNTs (carbon nanotubes) over a Riga sheet. The energy analysis is debated with the availability of radiation, viscous dissipation, and convective heating conditions. Two divisions of CNTs, like, SWCNTs (single-wall carbon nanotubes) and MWCNTs (multiwall carbon nanotubes), are considered. The pertinent variables are applied to overhaul the governing mathematical models into ODE expressions. The overhaul expressions are analytically solved by HAM (homotopy analysis method) and numerically solved by MATLAB bvp4c scheme. The repercussions of relevant parameters on nanoliquid velocity, nanoliquid temperature, skin friction coefficient, and local Nusselt number are inspected via graphs, tables, and charts. Our computational results are compared with the previous researcher results and have the most acceptable agreement. Our outcomes are used to understand the flow attributes, behavior, and how to predict it for those working in the design of thermal equipment in thermal industry. It is noticed that the nanoliquid velocity decayed in counter to the unsteady parameter, and it enhances for larger values of Hartmann number. The nanoliquid temperature enriches when raising the Biot number and radiation parameter. The change in unsteady parameter decays the surface shear stress, while reverse results are found in the local Nusselt number.

1. Introduction

In recent decades, enhancing the rate of liquid thermal transport in classical base liquids (engine oil, water, polymer-based solutions) has been a crucial challenge for modern researchers and technologists. One approach to enrich the liquid thermal conductivity is to mix nanometer size metallic particles (carbides, fullerene, oxides, nitrides, metals, and carbon nanotubes) with the classical base liquids. Carbon nanotubes are cylindrical format tubes with precious attributes such as robust thermal conductivity and enormous energy. These CNTs are segregated into SWCNTs (single-wall carbon nanotubes) and MWCNTs (multiwall carbon nanotubes) and are highly used in many industrial processes, like, drug delivery, nanotube transistors, micro-

wave amplifiers, pancreatic cancer test, and optics. Haq et al. [1] noted that the higher surface shear stress attains in engine oil-based CNTs compared to ethylene glycol-based CNTs in their MHD flow of CNTs over a stretching surface. The consequences of gasoline oil-based hybrid CNTs past a curved stretched surface by Muhammad et al. [2], and noticed that the nanoliquid velocity enhances for enriching both CNTs volume fractions. Gholinia et al. [3] proved that the nanoliquid temperature for SWCNTs is larger than the MWCNTs for the problem of the 3D flow of hybrid nanoliquids on a cylinder. They utilize ethylene glycol, water, and engine oil which are the base fluids. The 3D flow of carbon nanotubes past a variable ticked stretching surface was employed by Imtiaz et al. [4]. They concluded that the nanoliquid flow improves when increasing

$$V = V_w = \frac{ax}{1 - \xi t}; \qquad W = -\frac{W_0}{\sqrt{1 - \xi t}}; \qquad -k_{nf} T_y = h_c[T_f - T]$$
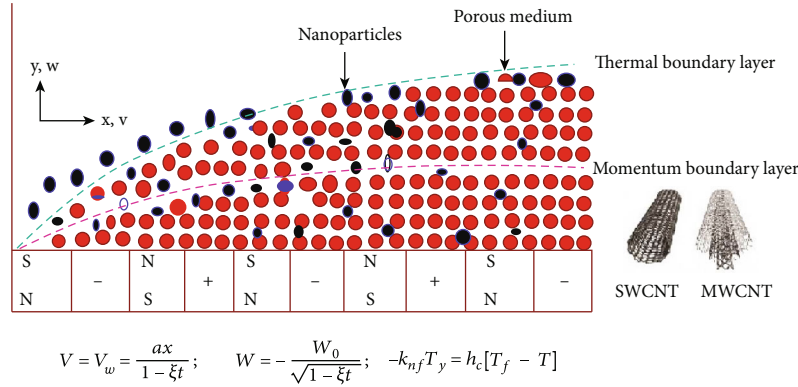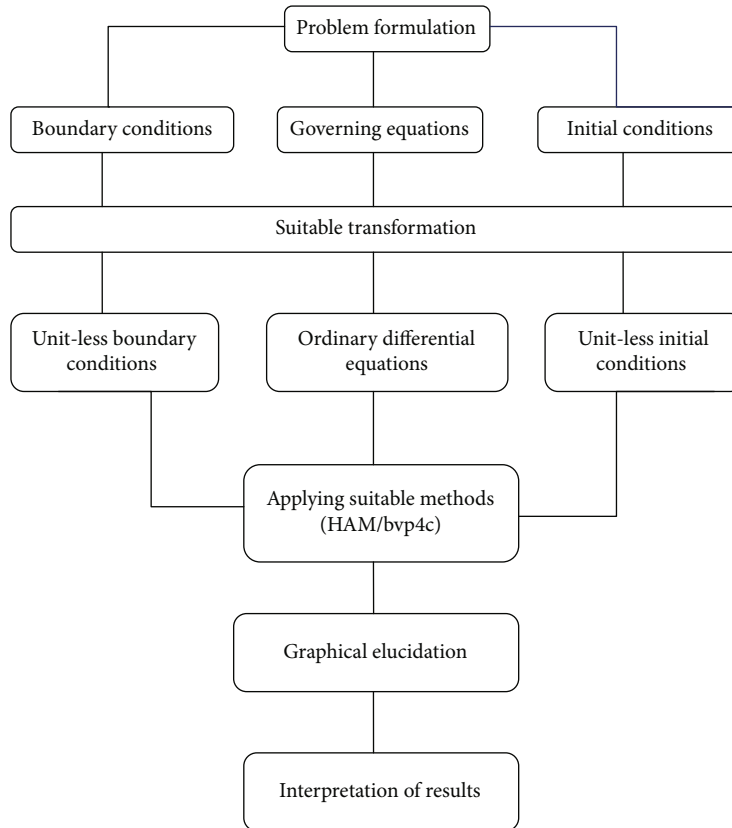
Figure 1: Physical configuration of the flow model.

Figure 2: Flow chart.

the nanoparticle shape factor. Anuar et al. [5] proved that the 5% quantity of volume fraction on water-based CNTs increases the heat transfer gradient up to 26% for the case of MHD flow of water-based CNTs past a nonuniform stretching surface. The time-dependent flow of Maxwell nanoliquid suspended with CNTs with four different base fluids was numerically investigated through Laplace transform technique by Aman et al. [6]. Anuar et al. [7] concluded that the strengthening of nanoparticle volume fraction is noted to enrich the heat transfer attributes on the surface in a flow of CNTs in an exponentially shrinking/stretching sheet. Heat transfer evaluation for Blasius flow of water/ethylene glycol-based CNTs over a plane plate

was disclosed by Ferdows et al. [8]. They detected that the MWCNTs have less heat transfer than SWCNTs.

Flow through porous space plays a notable role in many areas of biomedical engineering, pharmaceuticals, environmental engineering, crude oil production, spacecraft, etc. Many researchers are used extensively to model the flow through Darcy's law. But this law is applicable only for low velocity and low porosity cases. Also, this law is ineffectual when there is a larger flow speed and inconsistent porosity. Forchheimer [9] overcome this restriction to add a square velocity factor in the Darcian model. Later, this new model was called the Darcy-Forchheimer flow model (DFFM). Shafiq et al. [10] noticed that the Forchheimer

(a)

(b)
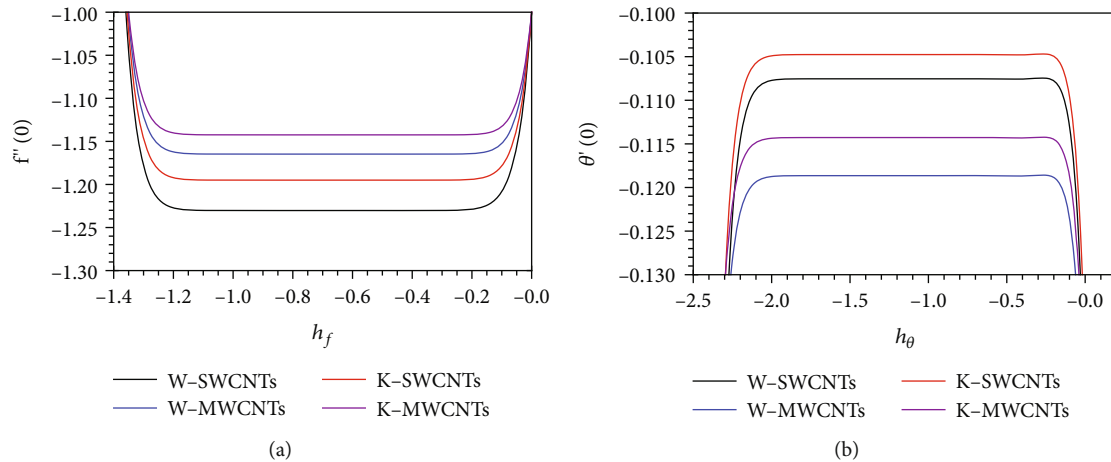
FIGURE 3: h-curves.

number upshots the nanoliquid flow in 3D Darcy-Forchheimer flow of nanoliquid in a rotating frame. The Darcy-Forchheimer flow of 3D nanoliquid with bioconvection and the activation energy was demonstrated by Tayyab et al. [11]. They acknowledged that the larger quantity of porosity parameter deteriorates the nanoliquid velocity and it improves the nanoliquid temperature. Alzahrani and Khan [12] proved that the Forchheimer number leads to the decay of the speed of working fluid in a mixed convective flow of nanoliquid with the Darcy-Forchheimer law. The Darcy-Forchheimer flow of hybrid nanoliquid in a rotating disk with first order velocity slip condition was analyzed by Haider et al. [13]. They detected that the porosity parameter leads to improving the skin friction coefficient. Alzahrani [14] is used as the optimal homotopy analysis method for solving the problem of 3D Darcy-Forchheimer flow of water-based CNTs subject to homogeneous- heterogeneous chemical reactions. The forced convective and stagnation-point flow of viscous liquid in a Forchheimer porous medium past a shrinking sheet was illustrated by Bakar et al. [15].

Nowadays, many researchers have been interested in analyzing the viscous dissipation impact because of its numerous industrial usages, like, as the design of electric ovens, paper creation, and crystal production. Pal et al. [16] proved that the heat transfer gradient declined for the presence of Eckert number to study the MHD flow of nanoliquid in a heated sheet with viscous dissipation. The MHD and Ohmic dissipative flow of Maxwell liquid on a stretching sheet with the available of thermal radiation was numerically addressed by Hsiao [17]. Their study proved that the mass transfer gradient grows when the Eckert number rises. Butt et al. [18] studied the impact of viscous dissipation and MHD flow of viscous liquid with entropy generation past a cylinder inserted in a porous medium. They detected that the Eckert number leads to improve the thickness of the thermal boundary layer. Alshehri and Shah [19] numerically analyzed the problem of the viscous dissipative flow of a hybrid nanoliquid with radiation. They detected that the nanoliquid thermal field improves when enhancing the Eckert number. Tang et al. [20] proved that the Eckert number

TABLE 1: Thermo-physical properties.

Physical characteristics	SWCNTs	MWCNTs	Kerosene	Water
k	6600	3000	0.145	0.613
ρ	2600	1600	783	997.1
cp	425	796	2090	4179

TABLE 2: Comparison of $-f''(0)$ for distinct values of fw with $A = \lambda = \phi = Fr = Ha = 0$ to Ibrahim and Shankar [44].

fw	Present study	Ref. [44]
0	1.000000	1.0000
0.5	1.280776	1.2808

leads to an upswing in the liquid temperate in their study of Sisko nanoliquid suspended with Au nanoparticles. The entropy optimization of Powell-Eyring nanoliquid with viscous dissipation impact was scrutinized by Rooman et al. [21], and they also see that the liquid warmness escalates when improving the Eckert number values. Further researches include, the viscous dissipative flow of hybrid nanoliquid by Muhammad et al. [22], nanoliquid and Casson liquid by Gopal et al. [23, 24], Powell-Eyring hybrid nanoliquid by Aziz et al. [25], blood-gold Carreau nanoliquid and dusty liquid by Koriko et al. [26], and dusty hybrid nanoliquid by Mallikarjuna et al. [27].

The outcomes of heat source/sink acquire an essential role in many industrial processes, like, foodstuffs storage, packed bed reactors, rubber sheets production, disposal of radioactive waste material, and thermal cooling systems. Sharma and Gandhi [28] reported that the larger temperature-dependent heat source/sink parameter improves the nanoliquid temperature in their time-dependent MHD viscous liquid flow with nonuniform heat source/sink and Joule heating. The flow of dusty liquid past a stretching sheet under the influence of a nonuniform heat sink/source was scrutinized by Gireesha et al. [29]. They revealed that the temperature-dependent heat sink/source parameter leads to strengthening the wall

TABLE 3: Order of approximations.

| Order | Water | | | | Kerosene | | | |
| | SWCNTs | | MWCNTs | | SWCNTs | | MWCNTs | |
	$-f''(0)$	$-\theta'(0)$	$-f''(0)$	$-\theta'(0)$	$-f''(0)$	$-\theta'(0)$	$-f''(0)$	$-\theta'(0)$
1	1.19741	0.11416	1.15346	0.12244	1.2243	0.10509	1.13688	0.11677
5	1.23027	0.11255	1.16476	0.12319	1.27562	0.10176	1.14243	0.11830
10	1.23026	0.11242	1.16474	0.12300	1.27568	0.10165	1.14241	0.11809
12	1.23026	0.11242	1.16474	0.12300	1.27568	0.10166	1.14241	0.11809
15	1.23026	0.11242	1.16474	0.12300	1.27568	0.10166	1.14241	0.11809
20	1.23026	0.11242	1.16474	0.12300	1.27568	0.10166	1.14241	0.11809
25	1.23026	0.11242	1.16474	0.12300	1.27568	0.10166	1.14241	0.11809
30	1.23026	0.11242	1.16474	0.12300	1.27568	0.10166	1.14241	0.11809
35	1.23026	0.11242	1.16474	0.12300	1.27568	0.10166	1.14241	0.11809

TABLE 4: The fluctuations of SFC of water-based SWCNTs and MWCNTs for distinct values of A, Ha, Fr, λ, and fw.

| A | Ha | Fr | λ | fw | SWCNTs | | MWCNTs | |
					HAM	Numerical	HAM	Numerical
0	0.5	0.4	0.2	0.4	−1.48806	−1.48806	−1.40807	−1.40806
0.3					−1.60099	−1.60099	−1.51573	−1.51574
0.7					−1.74581	−1.74581	−1.65380	−1.65380
1					−1.84908	−1.84908	−1.75233	−1.75233
0.3	0	0.4	0.2	0.4	−1.84060	−1.84060	−1.75824	−1.75824
	0.3				−1.69589	−1.69589	−1.61180	−1.61180
	0.7				−1.50723	−1.50723	−1.42078	−1.42078
	1				−1.36849	−1.36849	−1.28025	−1.28025
0.3	0.5	0	0.2	0.4	−1.46607	−1.46607	−1.38680	−1.38680
		0.5			−1.63313	−1.63313	−1.54645	−1.54645
		1			−1.78576	−1.78576	−1.69234	−1.69234
		1.5			−1.92701	−1.92695	−1.82738	−1.82732
0.3	0.5	0.4	0	0.4	−1.48098	−1.48098	−1.39054	−1.39054
			0.2		−1.60099	−1.60099	−1.51573	−1.51574
			0.4		−1.71237	−1.71237	−1.63130	−1.63130
			0.6		−1.81677	−1.81677	−1.73919	−1.73919
0.3	0.5	0.4	0.2	−0.6	−1.12169	−1.12169	−1.07830	−1.07830
				−0.3	−1.24519	−1.24519	−1.19186	−1.19186
				0	−1.38562	−1.38562	−1.32019	−1.32019
				0.3	−1.54406	−1.54406	−1.46417	−1.46417
				0.6	−1.72107	−1.72107	−1.62427	−1.62427

temperature gradient. Elgazery [30] inspected the time-dependent 2D flow of nanoliquid past a stretching sheet with a nonuniform heat source/sink and inclined magnetic field. They obtained that the heat transfer gradient aggravates for a higher magnitude of the heat sink parameter, whereas it subsides when improving the heat source parameter. The impact of inconsistent heat source/sink of the 3D flow of Fe_3O_4/Al_2O_3 nanoparticles past a Riga plate was studied by Ragupathi et al. [31]. They have seen that the heat source

parameter develops the thermal boundary layer thickness. Sandhyarani et al. [32] noted that the heat sink/source parameter declines the heat transfer gradient for the problem of stagnation and MHD flow of Williamson liquid past a sheet with an inconsistent heat sink/source. The heat transport analysis of the nonlinear radiative flow of Carreau and Casson liquid on a heated stretching surface with a nonuniform heat source/sink and magnetic dipole was investigated by Mahanthesh et al. [33].

TABLE 5: The fluctuations of SFC of kerosene-based SWCNTs and MWCNTs for distinct values of A, Ha, Fr, λ, and fw.

A	Ha	Fr	λ	fw	SWCNTs		MWCNTs	
					HAM	Numerical	HAM	Numerical
0	0.5	0.4	0.2	0.4	−1.54358	−1.54358	−1.38085	−1.38085
0.3					−1.66010	−1.66010	−1.48668	−1.48668
0.7					−1.80950	−1.80950	−1.62241	−1.62241
1					−1.91599	−1.91599	−1.71930	−1.71930
0.3	0	0.4	0.2	0.4	−1.89783	−1.89783	−1.73023	−1.73023
	0.3				−1.75423	−1.75423	−1.58317	−1.58317
	0.7				−1.56710	−1.56710	−1.39130	−1.39130
	1				−1.42953	−1.42953	−1.25012	−1.25012
0.3	0.5	0	0.2	0.4	−1.52112	−1.52112	−1.35982	−1.35982
		0.5			−1.69320	−1.69320	−1.51690	−1.51691
		1			−1.85040	−1.85040	−1.66046	−1.66046
		1.5			−1.99587	−1.99582	−1.79335	−1.79329
0.3	0.5	0.4	0	0.4	−1.54340	−1.54340	−1.35960	−1.35960
			0.2		−1.66010	−1.66010	−1.48668	−1.48668
			0.4		−1.76877	−1.76877	−1.60376	−1.60376
			0.6		−1.87089	−1.87090	−1.71288	−1.71288
0.3	0.5	0.4	0.2	−0.6	−1.15102	−1.15102	−1.06321	−1.06321
				−0.3	−1.28152	−1.28152	−1.17343	−1.17343
				0	−1.43053	−1.43053	−1.29771	−1.29771
				0.3	−1.59932	−1.59932	−1.43689	−1.43689
				0.6	−1.78848	−1.78848	−1.59140	−1.59140

The innovation of this analysis is estimating the unsteady and Darcy-Forchheimer flow of water/kerosene-based CNTs over a Riga plate subjected to nonlinear heat sink/source and thermal radiation impacts. In many industries depends on the heating/cooling of the surfaces, the existence of convective heat interchange between surrounding liquid and plate surface cannot be spurned because this type of flow model is a crucial role in many industrial processes, like, cooling of the nuclear reactor, aerodynamic process, material drying, and design of thermal equipment. The following are the key objectives of the ongoing research:

(1) Extend the existing mathematical model to water/kerosene-based CNTs with viscous dissipation and nonlinear heat sink/source

(2) What are the impacts of physical parameters on nanoliquid flow distributions?

(3) How does the hybrid nanoliquid affect the heat transfer rates?

2. Mathematical Formulation

This analysis directs the 2D time-dependent Darcy-Forchheimer flow of CNTs over a Riga sheet. Here, water and kerosene as a base liquid and the heat transference phenomenon are conducted through thermal radiation. Furthermore, the viscous dissipation and nonlinear heat sink/source are also adapted into the energy expression. Let the $x-$ axis be kept along the plate and the $y-$ axis perpendicular to the plate. In our analysis, two types of CNTs, SWCNTs (single-wall carbon nanotubes) and MWCNTs (multiwall carbon nanotubes), are considered. The plate surface is warmed through the hot liquid with liquid temperature T_f, creating a heat transference coefficient h_c. Let T_w is the temperature of the plate while T_∞ is the ambient temperature such that $T_w > T_\infty$. The physical configuration of the flow model and flow chart are presented in Figures 1 and 2. The governing nanoliquid model under the above presumption can be expressed as follows, see Pal et al. [16], Madhukesh et al. [34], and Chaudhary and Kanika [35]:

$$V_x + W_y = 0. \tag{1}$$

$$V_t + V V_x + W V_y = \nu_{nf} V_{yy} - \frac{\nu_{nf}}{k_1^*} V - \frac{c_b}{\sqrt{k_1^*}} V^2 + \frac{\pi J_0 M}{8 \rho_{nf}} Exp\left[-\frac{\pi}{a_1} V\right]. \tag{2}$$

Table 6: The fluctuations of LNN of water-based SWCNTs and MWCNTs for distinct values of R, Ec, AA, BB, and Bi.

R	Ec	AA	BB	Bi	SWCNTs		MWCNTs	
					HAM	Numerical	HAM	Numerical
0	0.5	0.1	0.1	0.5	0.32597	0.32597	0.33559	0.33559
1					0.47797	0.47797	0.50045	0.50045
2					0.62790	0.62790	0.66265	0.66265
3					0.77539	0.77539	0.82186	0.82186
0.4	0	0.1	0.1	0.5	0.52981	0.52981	0.53593	0.53593
	0.3				0.44411	0.44411	0.45546	0.45546
	0.6				0.35840	0.35840	0.37499	0.37499
	0.9				0.27270	0.27270	0.29452	0.29452
0.4	0.5	0	0.1	0.5	0.39878	0.39878	0.41217	0.41217
		0.2			0.37516	0.37516	0.39145	0.39145
		0.4			0.35153	0.35153	0.37074	0.37074
		0.6			0.32790	0.32790	0.35002	0.35002
0.4	0.5	0.1	0		0.39122	0.39122	0.40518	0.40518
			0.2		0.38244	0.38243	0.39826	0.39825
			0.4		0.37232	0.37231	0.39051	0.39050
			0.6		0.36033	0.35999	0.38172	0.38166
0.4	0.5	0.1	0.1	−1	−1.03704	−1.03715	−1.08198	−1.08222
				−0.5	−0.46577	−0.46577	−0.48501	−0.48501
				0	0	0	0	0
				0.5	0.38697	0.38697	0.40181	0.40181
				1	0.71358	0.71357	0.74011	0.74011

$$T_t + VT_x + WT_y$$
$$= \alpha_{nf}T_{yy} + \frac{16\sigma^*}{3k^*(\rho c_p)_{nf}}T_\infty^3 T_{yy} + \frac{\mu_{nf}}{(\rho c_p)_{nf}}V_y^2 \tag{3}$$
$$+ \frac{1}{(\rho c_p)_{nf}}\frac{k_{nf}V_w}{xv_{nf}}\left[AA(T_f - T_\infty)f' + (T - T_\infty)BB\right].$$

The corresponding boundary conditions are, see Chakraborty et al. [36] and Nandeppanavar and Shakunthala [37]:

$$V = V_w = \frac{ax}{1 - \xi t}\,;\, W = -\frac{W_0}{\sqrt{1 - \xi t}}\,;$$
$$-k_{nf}T_y = h_c\left[T_f - T\right] at\, y = 0, \tag{4}$$
$$V \longrightarrow 0\,;\, T \longrightarrow T_\infty\, as\, y \longrightarrow \infty.$$

All the flow variables are provided in the nomenclature part.

The thermophysical properties of CNTs are defined as:

$$\frac{\mu_{nf}}{\mu_f} = \frac{1}{(1 - \phi)^{2.5}}\,;\, \frac{\rho_{nf}}{\rho_f} = 1 - \phi + \phi\frac{\rho_{CNT}}{\rho_f}\,;$$
$$\frac{(\rho c_p)_{nf}}{(\rho c_p)_f} = 1 - \phi + \phi\frac{(\rho c_p)_{CNT}}{(\rho c_p)_f},$$

$$\alpha_{nf} = \frac{k_{nf}}{(\rho c_p)_{nf}}\,;\, \frac{k_{nf}}{k_f}$$
$$= \frac{1 - \phi + 2\phi(k_{CNT}/k_{CNT} - k_f)\,\ln\,(k_{CNT} + k_f/2k_f)}{1 - \phi + 2\phi(k_f/k_{CNT} - k_f)\,\ln\,(k_{CNT} + k_f/2k_f)}. \tag{5}$$

Define, see Haq et al. [1],

$$H = \sqrt{\frac{a}{v_f(1 - \xi t)}}y\,;\, V = \frac{a}{1 - \xi t}xf'(H)\,;$$
$$W = -\sqrt{\frac{av_f}{1 - \xi t}}f(H)\,;\, \theta = \frac{T - T_\infty}{T_f - T_\infty}. \tag{6}$$

Substituting Equation (6) in Equations ((2)–(3)), we have:

$$A_1A_2f'''(H) + f(H)f'(H) - \left[f'(H)\right]^2$$
$$- A\left[f'(H) + \frac{H}{2}f''(H)\right] - A_1A_2\lambda f'(H) \tag{7}$$
$$- Frf'(H)^2 + A_2HaExp[-\beta_R H] = 0.$$

TABLE 7: The fluctuations of LNN of kerosene-based SWCNTs and MWCNTs for distinct values of R, Ec, AA, BB, and Bi.

R	Ec	AA	BB	Bi	SWCNTs		MWCNTs	
					HAM	Numerical	HAM	Numerical
0	0.5	0.1	0.1	0.5	0.32698	0.32698	0.34215	0.34215
1					0.46553	0.46553	0.50074	0.50074
2					0.60288	0.60288	0.65726	0.65726
3					0.73863	0.73863	0.81139	0.81139
0.4	0	0.1	0.1	0.5	0.52677	0.52677	0.53571	0.53571
	0.3				0.44021	0.44021	0.45776	0.45776
	0.6				0.35365	0.35365	0.37981	0.37981
	0.9				0.26709	0.26709	0.30185	0.30185
0.4	0.5	0	0.1	0.5	0.39457	0.39457	0.41549	0.41549
		0.2			0.37044	0.37043	0.39609	0.39609
		0.4			0.34630	0.34630	0.37670	0.37670
		0.6			0.32216	0.32216	0.35730	0.35730
0.4	0.5	0.1	0	0.5	0.38685	0.38685	0.40877	0.40877
			0.2		0.37785	0.37785	0.40267	0.40267
			0.4		0.36743	0.36741	0.39593	0.39592
			0.6		0.35494	0.35437	0.38838	0.38835
0.4	0.5	0.1	0.1	−1	−0.98734	−0.98737	−1.06140	−1.06149
				−0.5	−0.45008	−0.45008	−0.48134	−0.48134
				0	0	0	0	0
				0.5	0.38250	0.38250	0.40579	0.40579
				1	0.71159	0.71159	0.75252	0.75253

$$\frac{A_3}{A_4}\frac{1}{\Pr}\theta''(H) + \frac{1}{\Pr A_4}\frac{4}{3}Rd\theta''(H) + f(H)\theta'(H) - f'(H)\theta(H)$$
$$+ \frac{A_1}{A_4}Ec\left[f''(H)\right]^2 - A\left[\theta(H) + \frac{H}{2}\theta'(H)\right]$$
$$+ \frac{A_3}{A_1 A_2 A_4}\frac{1}{\Pr}\left[AAf'(H) + BB\theta(H)\right].$$
(8)

The reduced boundary conditions are:

$$f(0) = fw \,; f'(0) = 1 \,; f'(\infty) = 0 \,;$$
$$\theta'(0) = -\frac{Bi}{A_3}\left[1 - \theta(0)\right]; \theta(\infty) = 0.$$
(9)

All the flow parameter details are provided in the nomenclature part.

Here:

$$A_1 = \frac{1}{(1-\phi)^{2.5}} \,;$$

$$A_2 = \frac{1}{\left(1 - \phi + \phi\left(\rho_{CNT}/\rho_f\right)\right)} \,;$$

$$A_3 = \frac{(1-\phi) + 2\phi(k_{CNT}/k_{CNT} - k_f) \ln\left(k_{CNT} + k_f/2k_f\right)}{(1-\phi) + 2\phi(k_f/k_{CNT} - k_f) \ln\left(k_{CNT} + k_f/2k_f\right)} \,;$$

$$A_4 = 1 - \phi + \phi\frac{(\rho c_p)_{CNT}}{(\rho c_p)_f}.$$
(10)

The skin friction coefficients and local Nusselt number are expressed as follows:

$$C_f\sqrt{\text{Re}} = A_1 f''(0) \,; \frac{Nu}{\sqrt{\text{Re}}} = -\left[A_3 + \frac{4}{3}Rd\right]\theta'(0).$$
(11)

3. Solution Methodology

3.1. Analytical Solution. The achieved ODE models, Equations ((7)–(8)) with the associated Condition (9) are solved analytically by exploiting HAM scheme. Liao created this scheme, see Liao [38]. This method is a potent mathematical technique for solving highly nonlinear problems, see Mabood et al. [39] and Dawar et al. [40].
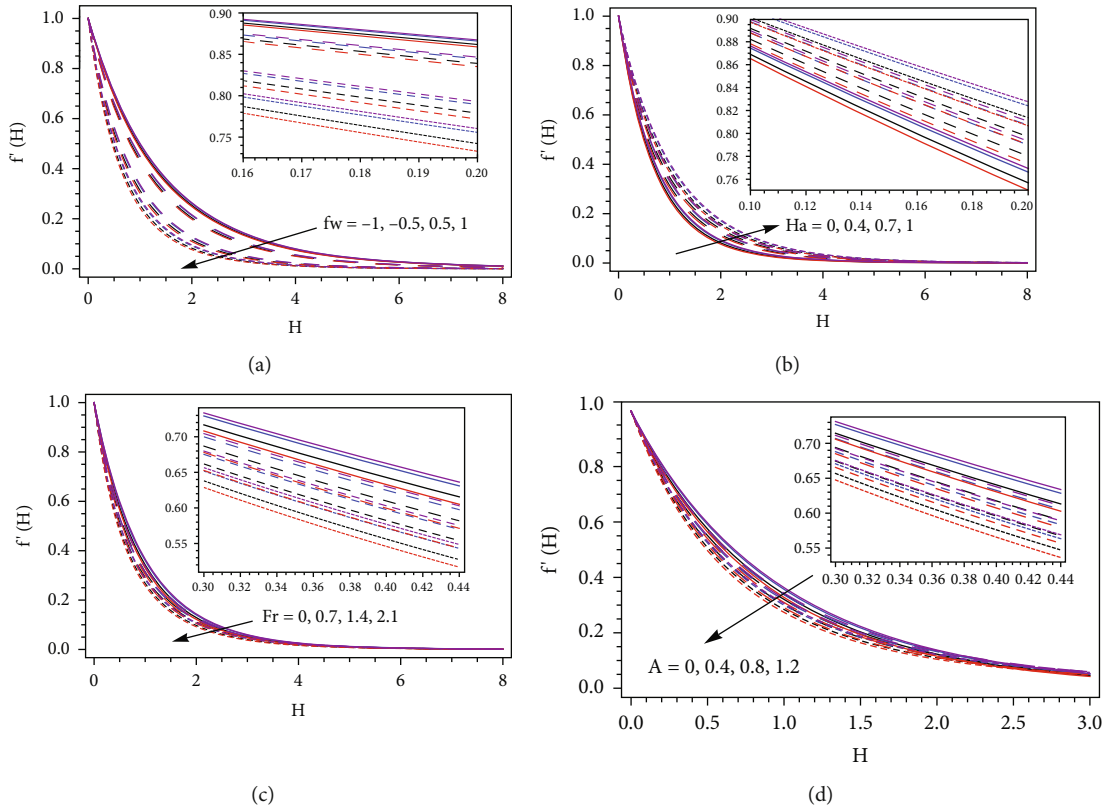
FIGURE 4: The impact of fw (a), Ha (b), Fr (c), and A (d) on $f'(H)$ for water-SWCNTs (black), water-MWCNTs (blue), glycerin-SWCNTs (red), and glycerin-MWCNTs (purple).
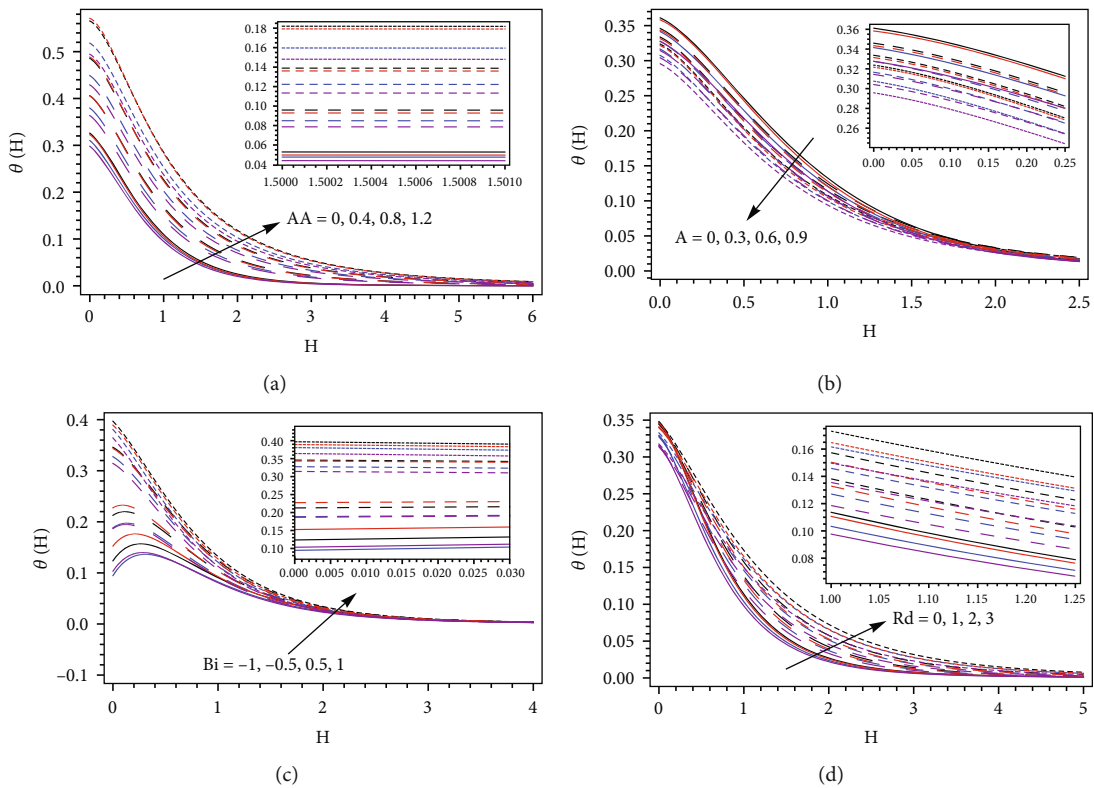

FIGURE 5: The impact of AA (a), A (b), Bi (c), and Rd (d) on $\theta(H)$ for water-SWCNTs (black), water-MWCNTs (blue), glycerin-SWCNTs (red), and glycerin-MWCNTs (purple).
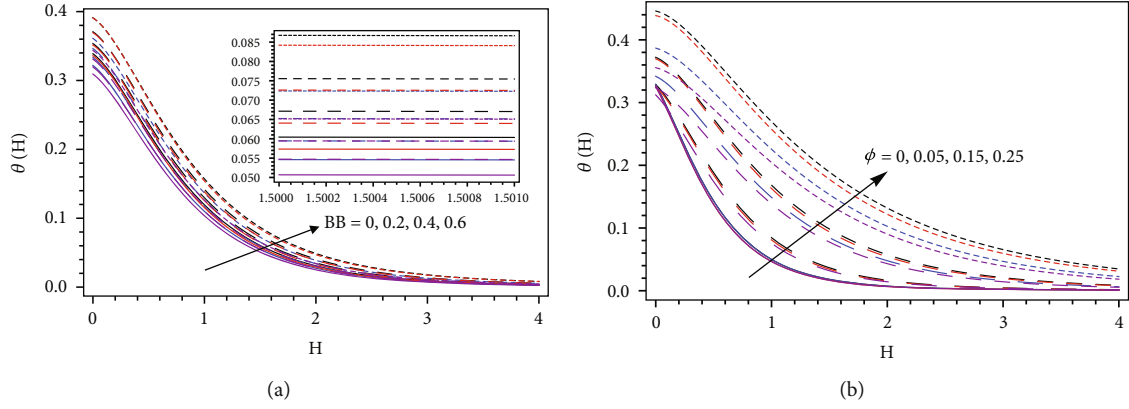
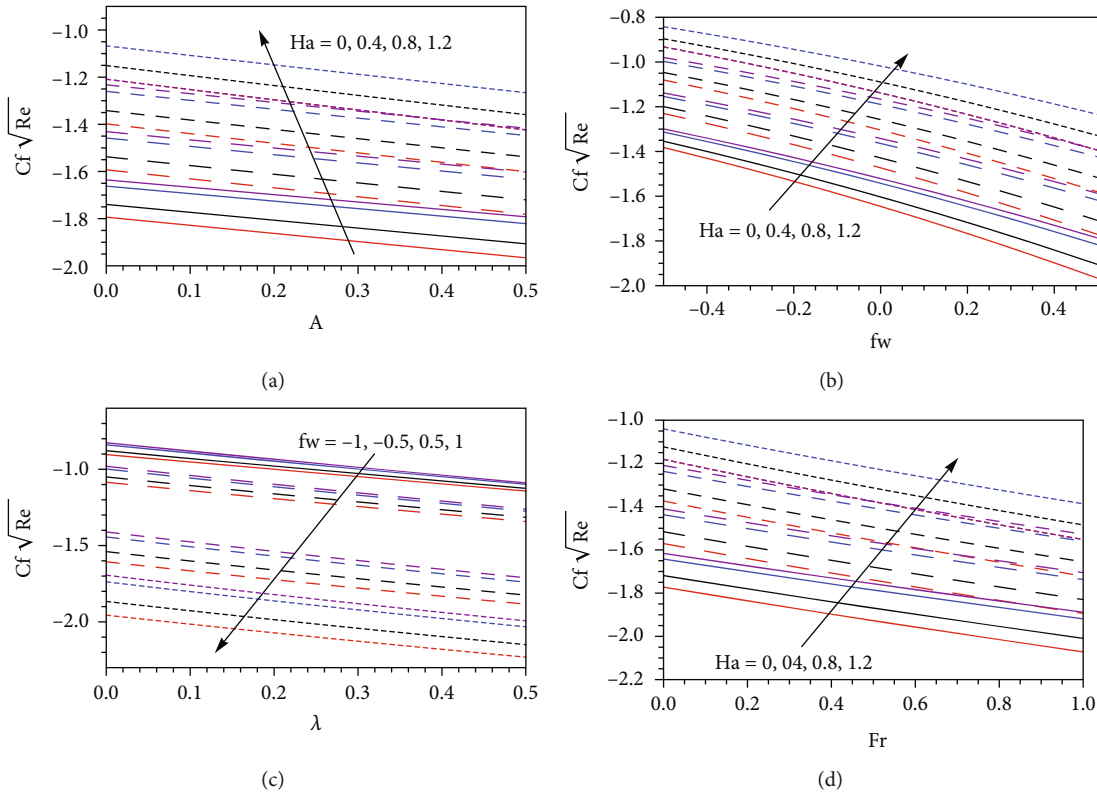FIGURE 6: The impact of BB (a) and ϕ (b) on $\theta(H)$ for water-SWCNTs (black), water-MWCNTs (blue), glycerin-SWCNTs (red), and glycerin-MWCNTs (purple).

FIGURE 7: The modifications of SFC for different combinations of Ha, A, fw, λ, and Fr for water-SWCNTs (black), water-MWCNTs (blue), glycerin-SWCNTs (red), and glycerin-MWCNTs (purple).

For this purpose, we fix the following initial approximation, linear operator and linear properties are $f(0) = fw + 1 - e^{-H}$; $\theta(0) = Bie^{-H}/(A_3 + Bi)$; $\pounds_f = f''' - f'$ and $\pounds_\theta = \theta'' - \theta$, and $\pounds_f[ß_1 + ß_2 e^H + ß_3 1/e^H] = 0 = \pounds_\theta[ß_4 e^H + ß_5 1/e^H]$, respectively, where $ß_j (j = 1 - 5)$ are constants. The zeroth-order deformation problems:

$$(1-q)\pounds_f[f(H,q) - f_0(H)] = qh_f M_1[f(H,q)]$$
$$(1-q)\pounds_\theta[\theta(H,q) - \theta_0(H)] = qh_\theta M_2[f(H,q), \theta(H,q)]$$

$$(12)$$

where $q \in [0, 1]$ is an embedding parameter and M_1 and M_2 are nonlinear operators.

After handling the nth order HAM, we acquire the following expressions:

$$f_n(H) = f_n^{\circledast}(H) + ß_1 + ß_2 e^H + ß_3 \frac{1}{e^H}.$$

$$\theta_n(H) = \theta_n^{\circledast}(H) + ß_4 e^H + ß_5 \frac{1}{e^H}.$$

$$(13)$$

where $f_n^{\circledast}(H)$ and $\theta_n^{\circledast}(H)$ are the particular solutions.
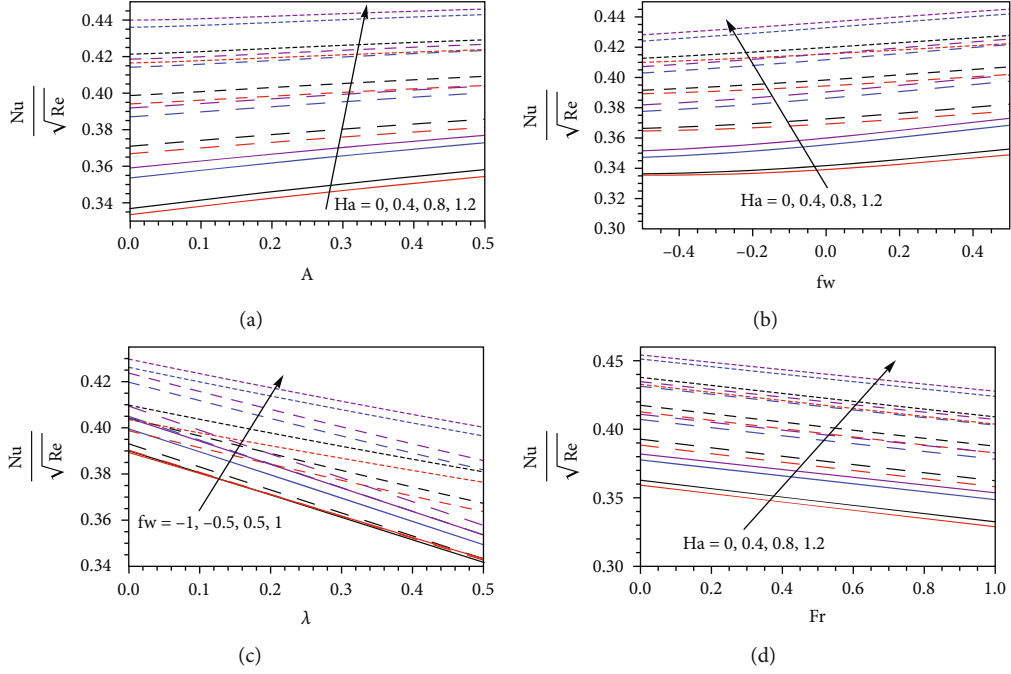
(a)

(b)

(c)

(d)

FIGURE 8: The modifications of LNN for different combinations of Ha, A, fw, λ, and Fr for water-SWCNTs (black), water-MWCNT s(blue), glycerin-SWCNTs (red), and glycerin-MWCNTs (purple).

The HAM parameters (h_f and h_θ) are the authoritative for solution convergent, see Prabakaran et al. [41] and Eswaramoorthi et al. [42]. The range values of h_f are [-1.2, -0.2] (W-SWCNTs), [-1.2,-0.2] (W-MWCNTs), [-1.2,-0.15] (K-SWCNTs), and [-1.2,-0.15] (K-MWCNTs) and the range values of h_θ are [-2, -0.3] (W-SWCNTs), [-2,-0.3] (W-MWCNTs), [-2,-0.29] (K-SWCNTs), and [-2,-0.29] (K-MWCNTs), collected in Figures 3(a) and 3(b) and fix $h_f = -0.7$ and $h_\theta = -1.2$ for better convergent.

3.2. Numerical Solution. The remodeled ODE Equations ((7)–(8)) with the corresponding boundary Condition (9) are solved numerically by applying MATLAB bvp4c procedure. In this regard, we convert the higher term into first-order equations, see Ali et al. [43]. Let $f = D_1, f' = D_2, f'' = D_3, \theta = D_4, \theta' = D_5.$

The system of equations are:

$$D_1' = D_2.$$

$$D_2' = D_3.$$

$$D_3' = \frac{D_2^2 - D_1 D_2 + A[D_2 + (H/2)D_3] + A_1 A_2 \lambda D_2 + Fr D_2^2 - A_2 Ha Exp[-\beta_R H]}{A_1 A_2}.$$

$$D_4' = D_5.$$

$$D_5' = \frac{D_2 D_4 - D_1 D_5 + A[D_4 + (H/2)D_5] - (A_1/A_4)Ec D_3^2 - (A_3/A_1 A_2 A_4)(1/Pr)[AAD_2 + BBD_4]}{(1/A_4 Pr)[A_3 + 4/3 Rd]}.$$

(14)

With the corresponding conditions:

$$D_1(0) = fw \, ; D_2(0) = 1 \, ; D_2(\infty) = 0 \, ;$$

$$D_5(0) = -\frac{B_i}{A_3}(1 - D_4(0)) \, ; D_4(\infty) = 0.$$

(15)

To solve the above problem by applying MATLAB bvp4c procedure with error is 10^{-5} and step size is 0.05.

4. Results and Discussion

The key role of this section is to examine the consequences of various pertinent parameters on nanoliquid velocity,
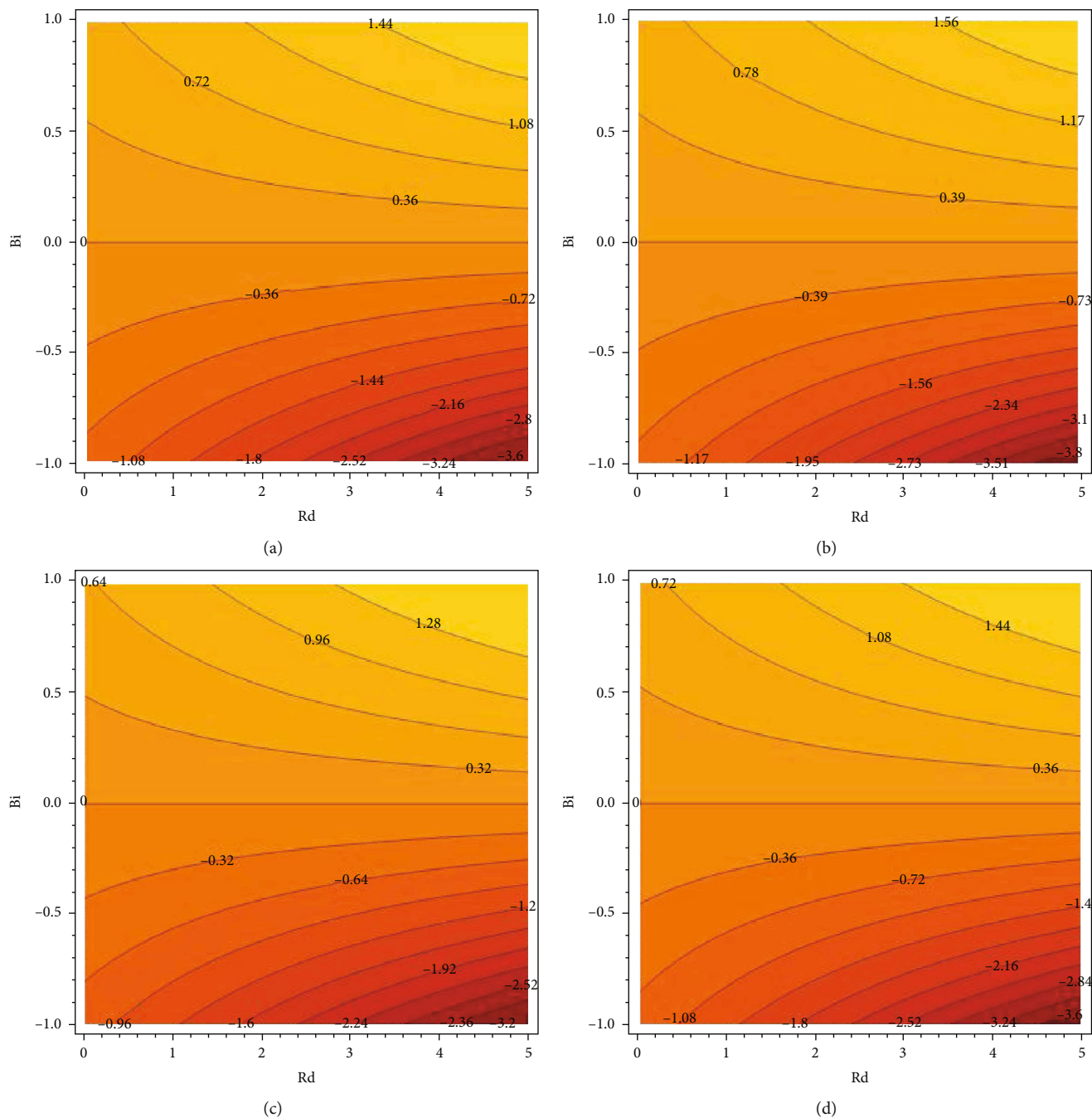
(a)

(b)

(c)

(d)

FIGURE 9: Stream line for Rd and Bi on LNN for water-SWCNTs (a), water-MWCNTs (b), glycerin-SWCNTs (c), and glycerin-MWCNTs (d).

nanoliquid temperature, skin-friction coefficient, and local Nusselt number for water/kerosene-based carbon nanotubes over a Riga plate. Table 1 provides the thermo-physical properties of SWCNTs, MWCNTs, kerosene, and water. Table 2 gives the comparison of $-f''(0)$ to Ibrahim and Shankar [44] for distinct values of fw with $A = \lambda = \phi = $ Fr $ = $ Ha $ = 0$ and found that our numerical results exactly matched with Ibrahim and Shankar [44]. The HAM order of approximations is illustrated in Table 3, and it is found that 12th order is sufficient for all computations. The fluctuations of

SFC of water and kerosene-based SWCNTs and MWCNTs for distinct values of A, Ha, Fr, λ, and fw are given in Tables 4 and 5. It is unveiled that the surface shear stress downturns when escalating the size of A, Fr, λ, and fw. However, it enhances for a larger quantity of Ha. In addition, the larger SFC attained in MWCNTs compared to the SWCNTs for both base liquids. Tables 6 and 7 were taken for the overview of the LNN of water and kerosene-based SWCNTs and MWCNTs for distinct values of R, Ec, AA, BB, and Bi. It is acknowledged that the higher amount of R and Bi leads to
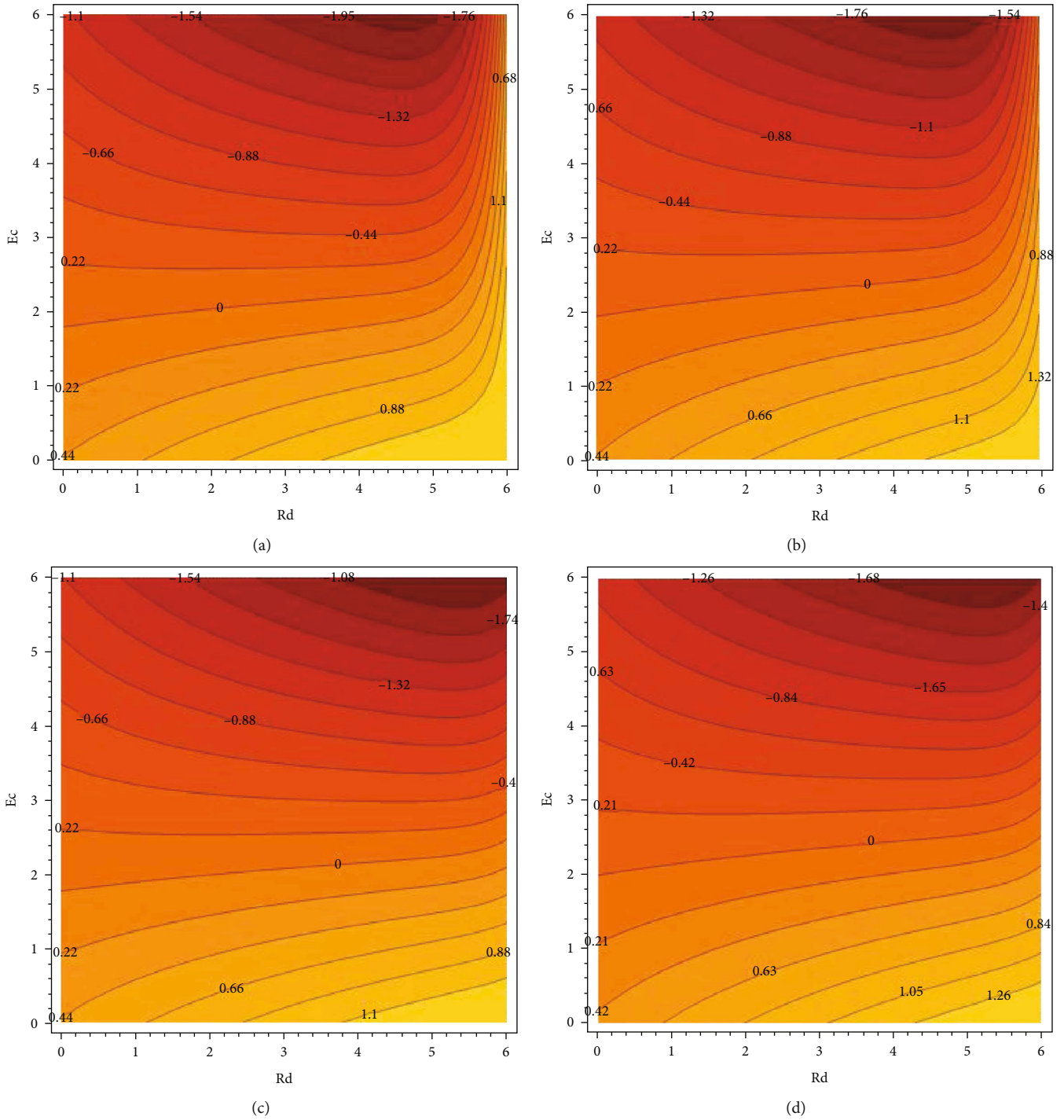
(a)

(b)

(c)

(d)

FIGURE 10: Stream line for Rd and Ec on LNN for water-SWCNTs (a), water-MWCNTs (b), glycerin-SWCNTs (c), and glycerin-MWCNTs (d).

develop the heat transfer gradient and Ec, AA, and BB deduce the heat transfer gradient.

Figures 4(a)–4(d) are drawn to show the upshot of fw, Ha, Fr, and A on nanoliquid velocity profile. It is evident from the outcomes that nanoliquid flow speed boosted up for larger Ha values while reverse measurements are found for positive changes of fw, Fr, and A. Physically, a bigger modified Hartmann number produces a greater electrical field, resulting in a larger wall-parallel Lorentz force. As a

result, the fluid velocity increases. To scrutiny, the significant's of AA, A, Bi, and Rd on nanoliquid temperature profile are drawn in Figures 5(a)–5(d), and it is found that nanoliquid temperature upturns when escalating the values of AA, Bi, and Rd, and it fallout when raising the quantity of A. Physically, the Biot number is related to the heat transfer coefficient. If the heat transfer coefficient is enhanced, the fluid temperature will rise. This is why enhancing the fluid temperature leads to a higher Biot number. Intensifying
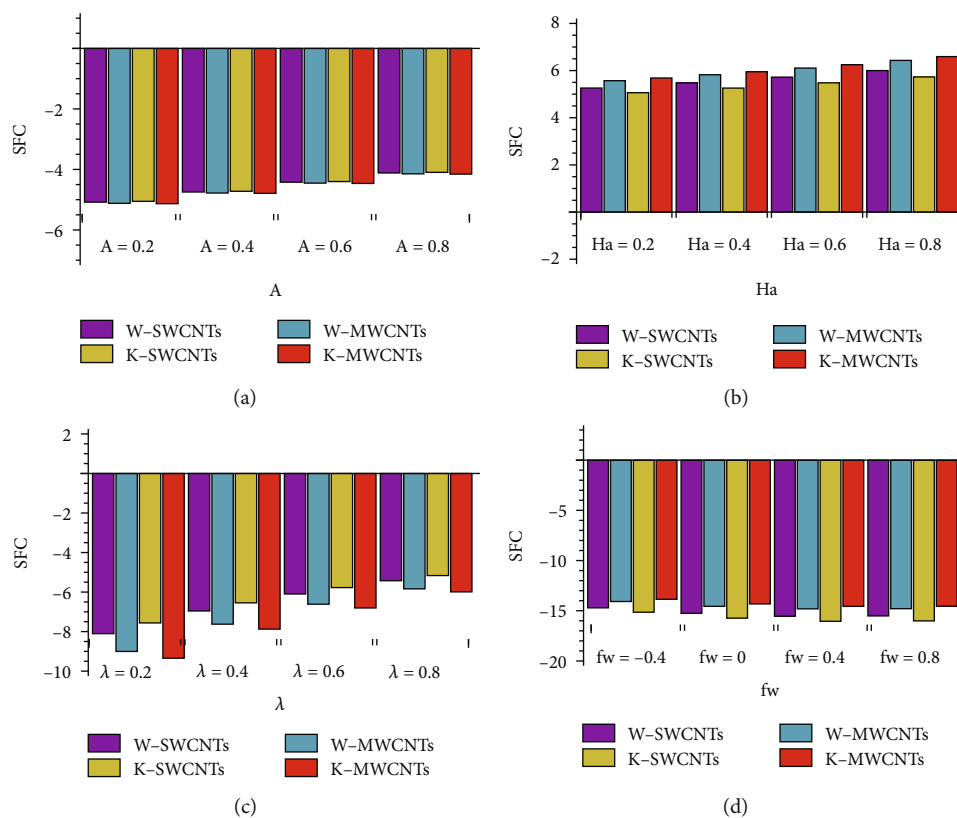
FIGURE 11: Growing/lessening percent of SFC on A (a), Ha (b), λ (c), and fw (d) for all cases.
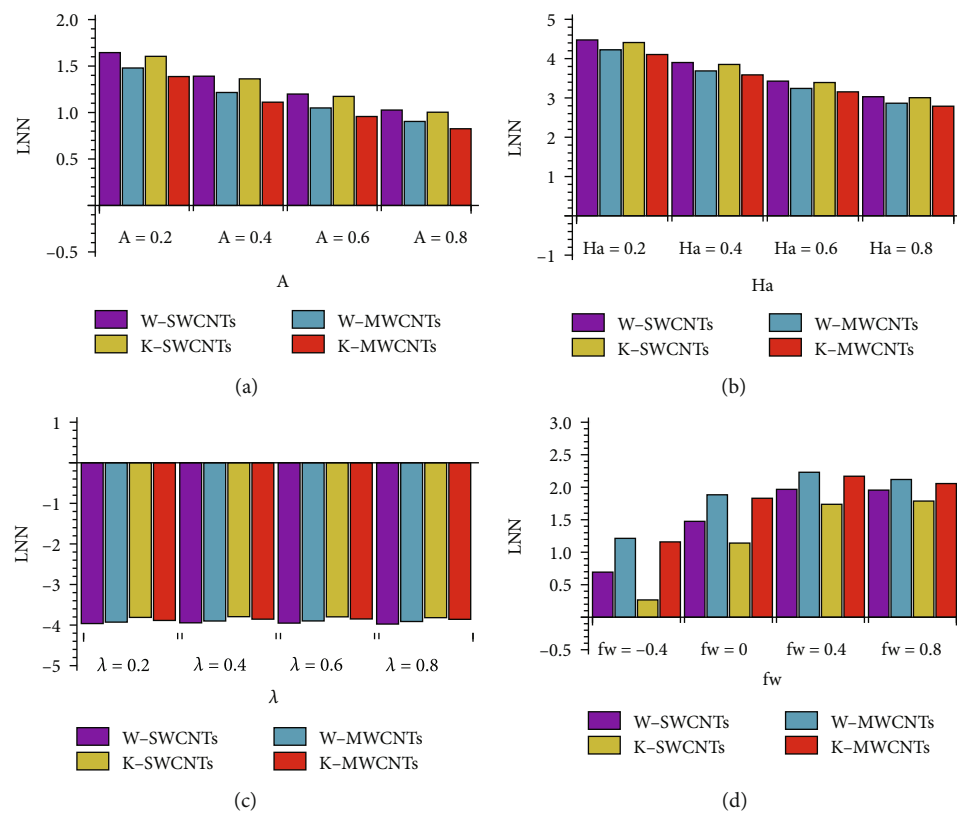

FIGURE 12: Growing/lessening percent of LNN on A (a), Ha (b), λ (c), and fw (d) for all cases.
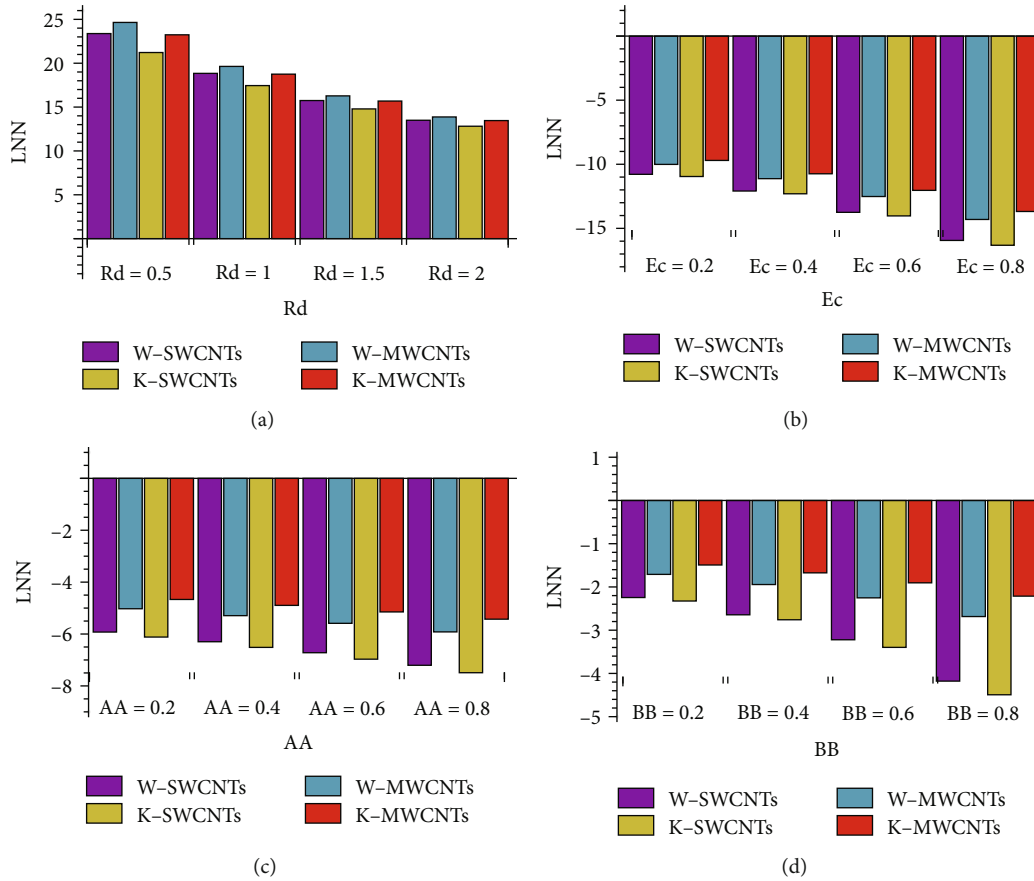
FIGURE 13: Growing/lessening percent of LNN on Rd (a), Ec (b), AA (c), and BB (d) for all cases.

the thermal radiation parameter accelerates the transfer of energy to the fluid. That is why the fluid's temperature is rising. Figures 6(a) and 6(b) are taken to inspect the affects of BB and ϕ on nanoliquid temperature profile. The results show that the nanoliquid becomes warmer when enriching the availability of BB and ϕ.

The modifications of SFC for different combinations of Ha, A, fw, λ, and Fr are draw in Figures 7(a)–7(d). It can be detected that plate surface shear stress improves when improving the modified Hartmann number while it suppresses for larger values of A, fw, λ, and Fr. Figures 8(a)–8(d) are presented to explain the impact of Ha, A, fw, λ, and Fr on local Nusselt number. It can be detected from these figures that the local Nusselt number escalates when heightening the quantity of Ha and A, and the opposite trend attains when rising the values of fw, λ, and Fr. The streamlines for both CNTs and both nanoliquids for the combinations of Rd and Bi and Rd and Ec are demonstrated in Figures 9(a)–9(d) and Figures 10(a)–10(d) for both cases.

Figures 11(a)–11(d) is drawn for to scrutinize the growing/lessening percent of SFC on A, Ha, λ, and fw for all cases. In the unsteady parameter case, the maximum lessening percentage (5.13%) appeared in kerosene-based MWCNTs when changing A from 0 to 0.2, and the minimum lessening percentage (4.10%) appeared in kerosene-based SWCNTs when changing A from 0.6 to 0.8. In the modified Hartmann case, the maximum growing percentage

(6.59%) appeared in kerosene-based MWCNTs when changing Ha from 0.6 to 0.8, and the minimum growing percentage (5.06%) appeared in kerosene-based SWCNTs when changing Ha from 0 to 0.2. In the porosity parameter case, the maximum lessening percentage (9.35%) appeared in kerosene-based MWCNTs when changing λ from 0 to 0.2, and the minimum lessening percentage (5.16%) appeared in kerosene-based SWCNTs when changing λ from 0.6 to 0.8. In the suction/injection parameter case, the maximum lessening percentage (16.05%) appeared in kerosene-based SWCNTs when changing fw from 0 to 0.4, and the minimum lessening percentage (13.86%) appeared in kerosene-based MWCNTs when changing fw from -0.8 to -0.4.

The growing/lessening percent of LNN on A, Ha, λ, and fw for all cases are deliberated in Figures 12(a)–12(d). In the unsteady parameter case, the maximum growing percentage (1.64%) appeared in water-based SWCNTs when changing A from 0 to 0.2, and the minimum growing percentage (0.83%) appeared in kerosene based MWCNTs when changing A from 0.6 to 0.8. In the modified Hartmann number case, the maximum growing percentage (4.75%) appeared in water-based SWCNTs when changing Ha from 0 to 0.2, and the minimum growing percentage (2.79%) appeared in kerosene based MWCNTs when changing Ha from 0.6 to 0.8. In the porosity parameter case, the maximum lessening percentage (3.98%) appeared in water-based SWCNTs when changing λ from 0.6 to 0.8, and the minimum

lessening percentage (3.79%) appeared in kerosene-based SWCNTs when changing λ from 0.2 to 0.4. In the suction/injection parameter case, the maximum growing percentage (2.23%) appeared in water-based MWCNTs when changing fw from 0 to 0.4, and the minimum growing percentage (0.27%) appeared in kerosene-based SWCNTs when changing fw from −0.8 to −0.4.

Figures 13(a)–13(d) is provide for to discuss the growing/lessening percent of LNN on Rd, Ec, AA, and BB for all cases. In the radiation parameter case, the maximum growing percentage (24.65%) appeared in water-based MWCNTs when changing Rd from 0 to 0.5, and the minimum growing percentage (12.82%) appeared in kerosene-based SWCNTs when changing Rd from 1.5 to 2. In the Eckert number case, the maximum lessening percentage (16.32%) appeared in kerosene-based SWCNTs when changing Ec from 0.6 to 0.8, and the minimum lessening percentage (9.70%) appeared in kerosene-based MWCNTs when changing Ec from 0 to 0.2. In the AA parameter case, the maximum lessening percentage (7.49%) appeared in kerosene-based SWCNTs when changing AA from 0.6 to 0.8, and the minimum lessening percentage (4.67%) appeared in kerosene-based MWCNTs when changing Å from 0 to 0.2. In the BB parameter case, the maximum lessening percentage (4.49%) appeared in kerosene-based SWCNTs when changing BB from 0.6 to 0.8, and the minimum lessening percentage (1.49%) appeared in kerosene-based MWCNTs when changing BB from 0 to 0.2.

5. Conclusions

The present communication provides the time-dependent 2D flow of water/kerosene-based carbon nanotubes over a Riga plate with thermal radiation, viscous dissipation, and convective heating conditions. The suitable variables are implemented to restructure the governing mathematical models into an ODE model. These models are analytically solved by the HAM (homotopy analysis method) and numerically solved by the MATLAB bvp4c scheme. The main observations are as follows:

(i) The larger modified Hartmann number corresponds to more nanoliquid velocity and the opposite reaction attained for larger values of the unsteady parameter

(ii) The nanoliquid velocity decays for the higher suction/injection parameter and Forchheimer number

(iii) The nanoliquid temperature develops because of enhancement of radiation parameter, Biot number, space-dependent, and temperature-dependent heat source/sink parameters

(iv) The plate surface shear stress depresses because of the Forchheimer number, unsteady parameter, and porosity parameter

(v) The heat transfer gradient enriches due to the more presence of suction/injection and Forchheimer number

(vi) In the future, we extend this work to nonFourier heat flux theory and slip effect

Nomenclature

a:	Positive constant
AA:	Space-dependent coefficient
α:	Thermal diffusivity
a_1:	Magnets positioned in the interval separating the electrodes
BB:	Temperature-dependent coefficient
C_f:	Skin-friction coefficient
c_p:	Capacity of specific heat
C_b:	Drag coefficient
h_c:	Heat transfer coefficient
J_0:	Current density applied to the electrodes
k:	Thermal conductivity
k^*:	Mean-absorption coefficient
k_1^*:	Permeability of the porous medium
M:	Magnetic property of the permanent magnets that are organized on top of on the plate surface
nf, f:	Subscript represents nanofluid and base fluid
ν:	Kinematic viscosity
H:	Dimensionless variable
ρ:	Density
T:	Nondimensional temperature
T_f:	Temperature of the hot fluid
T_w:	Surface temperature
T_∞:	Ambient temperature
θ:	Dimensionless temperature
V, W:	Velocity components
x, y:	Cartesian coordinates
$A(= \xi/a)$:	Unsteady parameter
$\mathrm{Bi}(= (h_c/k_f)\sqrt{\nu_f(1 - \xi t)/a})$:	Biot number
Ec:	Eckert number
$\beta(= (\pi/a_1)\sqrt{\nu_f(1 - \xi t)/a})$:	Dimensionless parameter
$Fr(= c_b x/\sqrt{k_1^*})$:	Forchheimer number
$\mathrm{fw}(= W_0/\sqrt{a\nu_f})$:	Suction/injection parameter
$\mathrm{Ha}(= \pi J_0 M/8\rho_f a^2 x)$:	Modified Hartmann number
$\lambda(= \nu_f/k_1^* a(1 - \xi t))$:	Porosity parameter
$\mathrm{Pr}(= \nu_f/\alpha_f)$:	Prandtl number
$\mathrm{Rd}(= 4\sigma^* T_\infty^3/k^* k_f)$:	Radiation parameter.

Data Availability

No data were used to support the findings of the study.

Conflicts of Interest

The authors declare that they have no competing interests.

Authors' Contributions

All authors contributed equally to this work. And all the authors have read and approved the final version manuscript.

References

[1] R. Ul Haq, S. Nadeem, Z. H. Khan, and N. F. M. Noor, "Convective heat transfer in MHD slip flow over a stretching surface in the presence of carbon nanotubes," *Physica B: Condensed Matter*, vol. 457, pp. 40–47, 2015.

[2] K. Muhammad, T. Hayat, A. Alsaedi, and B. Ahmed, "A comparative study for convective flow of basefluid (gasoline oil), nanomaterial (SWCNTs) and hybrid nanomaterial (SWCNTs+ MWCNTs)," *Applied Nanoscience*, vol. 11, no. 1, pp. 9–20, 2021.

[3] M. Gholinia, K. Hosseinzadeh, and D. Ganji, "Investigation of different base fluids suspend by CNTs hybrid nanoparticle over a vertical circular cylinder with sinusoidal radius," *Case Studies in Thermal Engineering*, vol. 21, article 100666, 2020.

[4] M. Imtiaz, F. Mabood, T. Hayat, and A. Alsaedi, "Impact of non-Fourier heat flux in bidirectional flow of carbon nanotubes over a stretching sheet with variable thickness," *Chinese Journal of Physics*, vol. 77, pp. 1587–1597, 2022.

[5] N. S. Anuar, N. Bachok, M. Turkyilmazoglu, N. Arifin, and H. Rosali, "Analytical and stability analysis of MHD flow past a nonlinearly deforming vertical surface in carbon nanotubes," *Alexandria Engineering Journal*, vol. 59, no. 1, pp. 497–507, 2020.

[6] S. Aman, I. Khan, Z. Ismail, M. Z. Salleh, and Q. M. Al-Mdallal, "Heat transfer enhancement in free convection flow of CNTs Maxwell nanofluids with four different types of molecular liquids," *Scientific Reports*, vol. 7, no. 1, p. 2445, 2017.

[7] N. S. Anuar, N. Bachok, N. Arifin, and H. Rosali, "Stagnation point flow and heat transfer over an exponentially stretching/shrinking sheet in CNT with homogeneous-heterogeneous reaction: stability analysis," *Symmetry*, vol. 11, no. 4, p. 522, 2019.

[8] M. Ferdows, M. D. Shamshuddin, S. O. Salawu, and M. Reza, "Computation of heat transfer in magnetised Blasius flow of nano-fluids with suspended carbon nanotubes through a moving flat plate," *International Journal of Ambient Energy*, pp. 1–9, 2022.

[9] P. Forchheimer, "Wasserbewegung durch boden," *Magazine Ver. D.Ing*, vol. 45, pp. 1782–1788, 1901.

[10] A. Shafiq, G. Rasool, and C. M. Khalique, "Significance of thermal slip and convective boundary conditions in three dimensional rotating Darcy-Forchheimer nanofluid flow," *Symmetry*, vol. 12, no. 5, p. 741, 2020.

[11] M. Tayyab, I. Siddique, F. Jarad, M. K. Ashraf, and B. Ali, "Numerical solution of 3D rotating nanofluid flow subject to Darcy-Forchheimer law, bio-convection and activation energy," *South African Journal of Chemical Engineering*, vol. 40, pp. 48–56, 2022.

[12] F. Alzahrani and M. I. Khan, "Analysis of Wu's slip and CNTs (single and multi-wall carbon nanotubes) in Darcy-Forchheimer mixed convective nanofluid flow with magnetic

[13] F. Haider, T. Hayat, and A. Alsaedi, "Flow of hybrid nanofluid through Darcy-Forchheimer porous space with variable characteristics," *Alexandria Engineering Journal*, vol. 60, no. 3, pp. 3047–3056, 2021.

[14] A. K. Alzahrani, "Darcy-Forchheimer 3D flow of carbon nanotubes with homogeneous and heterogeneous reactions," *Physics Letters A*, vol. 382, no. 38, pp. 2787–2793, 2018.

[15] S. A. Bakar, N. M. Arifin, R. Nazar, F. M. Ali, and I. Pop, "Forced convection boundary layer stagnation-point flow in Darcy-Forchheimer porous medium past a shrinking sheet," *Frontiers in Heat and Mass Transfer*, vol. 7, no. 1, 2016.

[16] D. Pal, D. Chatterjee, and K. Vajravelu, "Influence of magneto-thermo radiation on heat transfer of a thin nanofluid film with non-uniform heat source/sink," *Propulsion and Power Research*, vol. 9, no. 2, pp. 169–180, 2020.

[17] K. L. Hsiao, "Combined electrical MHD heat transfer thermal extrusion system using Maxwell fluid with radiative and viscous dissipation effects," *Applied Thermal Engineering*, vol. 112, pp. 1281–1288, 2017.

[18] A. S. Butt, A. Ali, and A. Mehmood, "Numerical investigation of magnetic field effects on entropy generation in viscous flow over a stretching cylinder embedded in a porous medium," *Energy*, vol. 99, pp. 237–249, 2016.

[19] A. Alshehri and Z. Shah, "Computational analysis of viscous dissipation and Darcy-Forchheimer porous medium on radioactive hybrid nanofluid," *Case Studies in Thermal Engineering*, vol. 30, article 101728, 2022.

[20] T.-Q. Tang, M. Rooman, N. Vrinceanu, Z. Shah, and A. Alshehri, "Blood flow of Au-nanofluid using Sisko model in stenotic artery with porous walls and viscous dissipation effect," *Micromachines*, vol. 13, no. 8, p. 1303, 2022.

[21] M. Rooman, M. A. Jan, Z. Shah et al., "Entropy optimization on axisymmetric Darcy-Forchheimer Powell-Eyring nanofluid over a horizontally stretching cylinder with viscous dissipation effect," *Coatings*, vol. 12, no. 6, p. 749, 2022.

[22] K. Muhammad, T. Hayat, and A. Alsaedi, "Numerical study of Newtonian heating in flow of hybrid nanofluid (SWCNTs +CuO+Ethylene glycol) past a curved surface with viscous dissipation," *Journal of Thermal Analysis and Calorimetry*, vol. 143, no. 2, pp. 1291–1302, 2021.

[23] D. Gopal, S. Saleem, S. Jagadha, F. Ahmad, A. O. Almatroud, and N. Kishan, "Numerical analysis of higher order chemical reaction on electrically MHD nanofluid under influence of viscous dissipation," *Alexandria Engineering Journal*, vol. 60, no. 1, pp. 1861–1871, 2021.

[24] D. Gopal, N. Kishan, and C. S. K. Raju, "Viscous and Joule's dissipation on Casson fluid over a chemically reacting stretching sheet with inclined magnetic field and multiple slips," *Informatics in Medicine Unlocked*, vol. 9, pp. 154–160, 2017.

[25] A. Aziz, W. Jamshed, T. Aziz, H. M. S. Bahaidarah, and K. U. Rehman, "Entropy analysis of Powell-Eyring hybrid nanofluid including effect of linear thermal radiation and viscous dissipation," *Journal of Thermal Analysis and Calorimetry*, vol. 143, no. 2, pp. 1331–1343, 2021.

[26] O. K. Koriko, K. S. Adegbie, N. A. Shah, I. L. Animasaun, and M. A. Olotu, "Numerical solutions of the partial differential equations for investigating the significance of partial slip due to lateral velocity and viscous dissipation: the case of blood-

dipole: Intelligent nano-coating simulation," *Materials Science and Engineering: B*, vol. 277, article 115586, 2022.

gold Carreau nanofluid and dusty fluid," *Numerical Methods for Partial Differential Equations*, pp. 1–29, 2021.

[27] H. B. Mallikarjuna, T. Nirmala, R. J. Punith Gowda, R. Manghat, and R. S. Varun Kumar, "Two-dimensional Darcy-Forchheimer flow of a dusty hybrid nanofluid over a stretching sheet with viscous dissipation," *Heat Transfer*, vol. 50, no. 4, pp. 3934–3947, 2021.

[28] B. K. Sharma and R. Gandhi, "Combined effects of Joule heating and non-uniform heat source/sink on unsteady MHD mixed convective flow over a vertical stretching surface embedded in a Darcy-Forchheimer porous medium," *Propulsion and Power Research*, vol. 11, no. 2, pp. 276–292, 2022.

[29] B. J. Gireesha, G. K. Ramesh, M. S. Abel, and C. S. Bagewadi, "Boundary layer flow and heat transfer of a dusty fluid flow over a stretching sheet with non-uniform heat source/sink," *International Journal of Multiphase Flow*, vol. 37, no. 8, pp. 977–982, 2011.

[30] N. S. Elgazery, "Nanofluids flow over a permeable unsteady stretching surface with non-uniform heat source/sink in the presence of inclined magnetic field," *Journal of the Egyptian Mathematical Society*, vol. 27, no. 1, 2019.

[31] P. Ragupathi, A. K. A. Hakeem, Q. M. Al-Mdallal, B. Ganga, and S. Saranya, "Non-uniform heat source/sink effects on the three-dimensional flow of Fe3O4 /Al2O3 nanoparticles with different base fluids past a Riga plate," *Case Studies in Thermal Engineering*, vol. 15, article 100521, 2019.

[32] B. Sandhyarani, M. Monica, and J. Anand Rao, "Effect of nonlinear thermal radiation on magnetohydrodynamic stagnation point flow of Williamson fluid induced by nonlinear stretching sheet in the presence of non uniform heat generation/absorption," *Journal of Nanofluids*, vol. 8, no. 7, pp. 1528–1534, 2019.

[33] B. Mahanthesh, I. L. Animasaun, M. R. Gorji, and I. M. Alarifi, "Quadratic convective transport of dusty Casson and dusty Carreau fluids past a stretched surface with nonlinear thermal radiation, convective condition and non-uniform heat source/sink," *Physica A: Statistical Mechanics and its Applications*, vol. 535, article 122471, 2019.

[34] J. K. Madhukesh, G. K. Ramesh, E. H. Aly, and A. J. Chamkha, "Dynamics of water conveying SWCNT nanoparticles and swimming microorganisms over a Riga plate subject to heat source/sink," *Alexandria Engineering Journal*, vol. 61, no. 3, pp. 2418–2429, 2022.

[35] S. Chaudhary and K. M. Kanika, "Radiation heat transfer on SWCNT and MWCNT based magnetohydrodynamic nanofluid flow with marangoni convection," *Physica Scripta*, vol. 95, no. 2, article 025202, 2020.

[36] T. Chakraborty, K. Das, and P. K. Kundu, "Framing the impact of external magnetic field on bioconvection of a nanofluid flow containing gyrotactic microorganisms with convective boundary conditions," *Alexandria Engineering Journal*, vol. 57, no. 1, pp. 61–71, 2018.

[37] M. M. Nandeppanavar and S. Shakunthala, "Impact of Cattaneo-Christov heat flux on magnetohydrodynamic flow and heat transfer of carbon nanofluid due to stretching sheet," *Journal of Nanofluids*, vol. 8, no. 4, pp. 746–755, 2019.

[38] S. Liao, *Homotopy analysis method in nonlinear differential equations*, Higher education press, 2012.

[39] F. Mabood, M. D. Shamsuddin, and S. R. Mishra, "Characteristics of thermophoresis and Brownian motion on radiative reactive micropolar fluid flow towards continuously moving flat plate: HAM solution," *Mathematics and Computers in Simulation*, vol. 191, pp. 187–202, 2022.

[40] A. Dawar, S. Islam, Z. Shah, S. R. Mahmuod, and S. A. Lone, "Dynamics of inter-particle spacing, nanoparticle radius, inclined magnetic field and nonlinear thermal radiation on the water-based copper nanofluid flow past a convectively heated stretching surface with mass flux condition: a strong suction case," *International Communications in Heat and Mass Transfer*, vol. 137, article 106286, 2022.

[41] R. Prabakaran, S. Eswaramoorthi, K. Loganathan, and I. E. Sarris, "Investigation on thermally radiative mixed convective flow of carbon $_{Nanotubes/Al2O3}$ nanofluid in water past a stretching plate with Joule heating and viscous dissipation," *Micromachines*, vol. 13, no. 9, p. 1424, 2022.

[42] S. Eswaramoorthi, K. Loganathan, R. Jain, and S. Gyeltshen, "Darcy-Forchheimer 3D flow of glycerin-based carbon nanotubes on a Riga plate with nonlinear thermal radiation and Cattaneo-Christov heat flux," *Journal of Nanomaterials*, vol. 2022, Article ID 5286921, 20 pages, 2022.

[43] F. Ali, K. Loganathan, S. Eswaramoorthi, K. Prabu, A. Zaib, and D. K. Chaudhary, "Heat transfer analysis on carboxymethyl cellulose water-based cross hybrid nanofluid flow with entropy generation," *Journal of Nanomaterials*, vol. 2022, Article ID 5252918, 11 pages, 2022.

[44] W. Ibrahim and B. Shankar, "MHD boundary layer flow and heat transfer of a nanofluid past a permeable stretching sheet with velocity, thermal and solutal slip boundary conditions," *Computers & Fluids*, vol. 75, pp. 1–10, 2013.